Implementation of a High-Performance GaN-Based Light-Emitting Diode Grown on a Nanocomb-Shaped Patterned Sapphire Substrate

Jian-Kai Liou, Chun-Chia Chen, Po-Cheng Chou, Zong-Jie Tsai, Yu-Chih Chang, and Wen-Chan Liu, *Senior Member, IEEE*

***Abstract*— A GaN-based light-emitting diode (LED) grown on a nanocomb-shaped patterned sapphire substrate (PSS) is fabricated and studied. Nanocomb-shaped patterns are transferred on a sapphire substrate using a well-ordered anodized aluminum oxide (AAO) thin film as a mask for the inductively coupled plasma etching process. This well-ordered AAO thin film with a high aspect ratio is grown on a sapphire substrate by an oxalic acid-based electrochemical system and a three-step anodization. The strain state generated during epitaxial growth could be effectively alleviated by the use of nanocomb-shaped PSS. The treading dislocation density could be reduced. Thus, the enhanced crystalline quality is obtained. In addition, due to the presence of photonic crystal-like air buffer layer, part of reflected photons upward the top side could be scattered by this layer. Therefore, more photons could be extracted outside. Experimentally, at 20 mA, as compared with a conventional LED grown on a planar sapphire substrate, the studied LED grown on a nanocomb-shaped PSS shows 53.8% and 43.7% enhancements in light output power and external quantum efficiency as well as a reduced leakage current.**

***Index Terms*— GaN, light-emitting diodes, patterned sapphire substrate, anodized aluminum oxide, nanocomb-shaped pattern, crystalline quality.**

I. Introduction

III-V COMPOUND materials play the important role in optoelectronic semiconductor devices such as solar cell, optoelectronic switch, laser, and light-emitting diode (LED) [1]–[4]. Recently, due to the great potential in solid-state lighting, interests in III-V compound GaN-based LEDs have been increased. As a promising light source, GaN-based LEDs could be extensively applied in many applications [5]. However, one of major challenges for the real application in solid-state lighting of GaN-based LEDs is low external quantum efficiency (EQE), which is limited by internal quantum efficiency (IQE) and light extraction efficiency (LEE) [6]. Due to the large lattice mismatch and difference in thermal expansion coefficients between GaN and sapphire, highly compressive stress, which is induced with the decrement of growth temperature during the epitaxial growth process, leads to many treading dislocations (TDs) ($10^8 \sim 10^{10}$ cm^{-2}) on GaN epitaxial layers. These TDs seriously reduce IQE and reliability [7]. Due to the large difference in refractive indices between GaN and air, LEE is constrained by the total internal reflection [6]. It is well known that patterned sapphire substrate (PSS) is one of effective methods to enhance EQE, because PSS could improve both IQE and LEE of GaN-based LEDs simultaneously [8]. Since PSS could restrict the presence of strain, the TD density could be reduced by the employment of PSS. This certainly leads to an improved IQE. On the other hand, PSS could also redirect the light path and increase the light scattering effect to cause a higher LEE [8]. Various patterns, such as hemispherical, conical, cylindrical, and pyramidal are employed in PSS to enhance the performance of GaN-based LEDs [9]. Although GaN-based LEDs with a convex PSS could exhibit the better crystal quality of GaN epitaxial layer than those with a concave PSS, it should be noted that the formation of air voids was also found in GaN-based LEDs with a concave PSS [10]. Due to the change of refractive indices, these air voids could reflect downward photons upward rather than be absorbed. It is known that reducing geometrical size of patterns from microscale to nanoscale could increase the number of patterns on PSS and result in enhanced light scattering effect [8]. In addition, a subwavelength-scale PSS with a well-ordered arrangement could also be regarded as a photonic crystal (PhC) structure, which could enhance light scattering effect or reflect photons as a photonic band gap [11].

Yet, only a few approaches have been applied to form nanoscale patterns, especially for the one with a well-ordered arrangement [8]. Due to high cost and low throughput of these complex nanofabrication approaches, nanoscale PSS could not be implemented in commercial products [12]. For this reason, a potentially alternative approach to form nanoscale pattern by the use of self-organized anodized aluminum oxide (AAO) film is studied. AAO has attracted much attention because of its interesting nanocomb structure, which exhibits high

Manuscript received August 21, 2014; revised October 20, 2014; accepted October 22, 2014. Date of publication October 27, 2014; date of current version November 4, 2014. This work was supported in part by the National Science Council of Taiwan under Contract NSC-101-2221-E-006-142-MY3, in part by the Ministry of Science and Technology, China, under Contract MOST-103-2221-E-006-244-MY3, and in part by the Advanced Optoelectronic Technology Center, National Cheng Kung University, Tainan, Taiwan.

The authors are with the Department of Electrical Engineering, Institute of Microelectronics, National Cheng Kung University, Tainan 70101, Taiwan (e-mail: q18001250@mail.ncku.edu.tw; q18001268@gmail.com; q18001276@mail.ncku.edu.tw; q16014029@mail.ncku.edu.tw; q16001107@mail.ncku.edu.tw; wcliu@mail.ncku.edu.tw).

Color versions of one or more of the figures in this paper are available online at http://ieeexplore.ieee.org.

Digital Object Identifier 10.1109/JQE.2014.2365022

aspect ratio and well-ordered hexagonal arrangement [13]. The nanocomb structure is a self-organized hexagonal arrangement with cylindrical pores of a variable diameter from 50 to 420 nm and a controlled depth depending on the employed anodizing condition [14]. An AAO thin film could be formed by simple electrochemical anodizations in various acidic electrolytes and exhibit advantages of inexpensive and high throughput [15]. Previously, a GaN-based LED grown on an AAO-nanoporous PSS was proposed to improve performance [13]. However, the mechanism of AAO thin film grown on a sapphire substrate and the comparison of device performance between GaN-based LEDs grown on nanoconvex-shaped and nanoconcave-shaped PSSs did not be addressed in detail. In this work, a large-area self-organized AAO thin film is successfully grown on a sapphire substrate by an oxalic acid-based electrochemical system. The anodization reaction procedures of AAO thin film grown on a sapphire substrate are also studied. The AAO thin film is then utilized as a hard mask to transfer nanocomb patterns on the sapphire substrate. A GaN-based LED grown on the nanocomb-shaped PSS is fabricated and demonstrated. Experimentally, the enhanced performance could be obtained.

II. Experimental

In this work, an AAO thin film was firstly grown on a planar sapphire substrate. The AAO growth approach could be mainly divided into two parts. The first part is anodization, and the other part is removal of alumina layer. A well-ordered AAO thin film could be formed by a multi-step anodization approach [16]. Hence, a three-step anodization approach was introduced to obtain a more orderly AAO thin film. Before AAO growth, the sapphire substrate was cleaned by acetone, hydrochloric acid, and deionized water sequentially. A 1μm-thick aluminum (Al) layer was then deposited on the cleaned sapphire substrate by a thermal evaporator. The Al layer was anodized under a DC operation voltage of 40 V in a 0.3 M oxalic acid solution at 4 °C for 3 minutes to eliminate large ridges and texture the surface of Al layer [16]. After the first anodization, the resulting alumina layer was removed by treating with a 0.5 M sodium hydroxide (NaOH) solution for 1 minute. Since alumina layer could be dissolved by a NaOH solution more rapidly as compared with the typical used phosphoric acid (H_3PO_4) solution, using a NaOH solution could significantly shorten the time required for the removal of alumina layer [20]. The second anodization was adopted under same conditions as the first anodization including the removal of alumina layer to create a highly ordered AAO thin film. Finally, the third anodization was carried out for 10 hours to increase the pore depth. After three-step anodization approach, the well-ordered AAO thin film was then utilized as an etching mask to transfer nanocomb patterns on the sapphire substrate by directly using an inductively coupled plasma (ICP) dry etching technique with a mixed ambience of Cl_2/Ar (30/10 sccm, 5 mtorr) and a source power of ICP/RIE (700W/120W) for 10 minutes. Subsequently, epitaxial layers of the studied device (denoted as the device C) were grown on the nanocomb-shaped PSS by a Thomas Swan

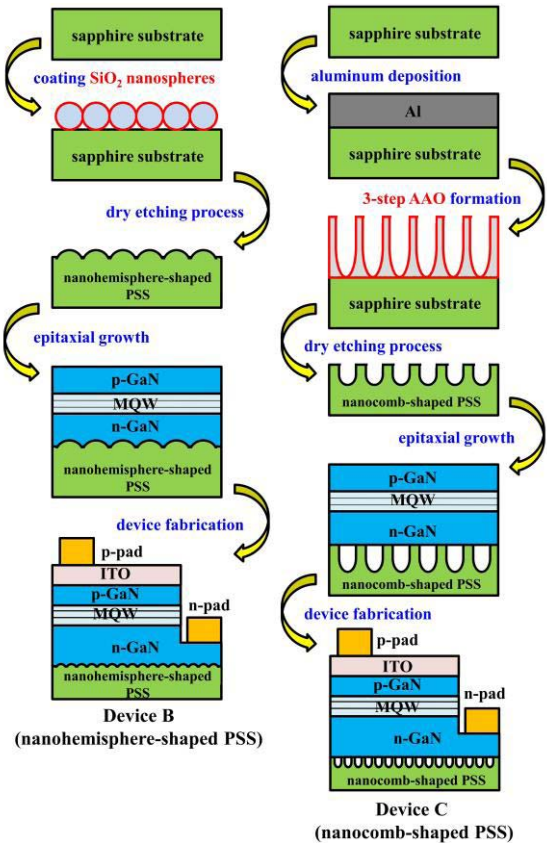

Fig. 1. Fabrication procedures and schematic diagrams of devices B and C.

metal-organic chemical vapor deposition (MOCVD) system. Details of the epitaxial structures for the studied devices were reported elsewhere [13]. After epitaxial growth, an ICP dry etching process was used again to define the mesa region. A 250 nm-thick indium-tin-oxide (ITO) layer was deposited as a current spreading layer and Cr/Pt/Au metals were sequentially deposited as n-p pads by an electron beam evaporator. Then, n-p pads were activated in a nitrogen ambience at 385 °C for 20 minutes to improve metal-semiconductor (MS) contact characteristics. It's known that a subwavelength scale should be adopted to form more PhC-like air voids [11]. To obtain a self-assembled SiO_2 nanosphere monolayer and a well-ordered AAO thin film on a sapphire substrate at the same time, sizes of these nanostructures around 100 nm are chosen in this work. For comparison, SiO_2 nanospheres with diameters of 100 $\pm$ 5 nm were drop-coated on a planar sapphire substrate to act as an etching mask and transfer convex nanohemisphere-shaped patterns. GaN-based LEDs grown on a planar sapphire substrate and a nanohemisphere-shaped PSS were then fabricated, and denoted as devices A and B, respectively. To limit the variation of epitaxial growth conditions, these three different substrates were loaded to finish epitaxial growth in the same run. Then, these wafers were diced into individual chips with a dimension of 254×585 μm^2. Figure 1 illustrates fabrication procedures and schematic diagrams of devices B and C. Finally, these chips were attached and bonded to TO-3 submounts for electrical and optical measurements. The electrical characteristics were measured by a semiconductor parameter analyzer (HP-4155C).

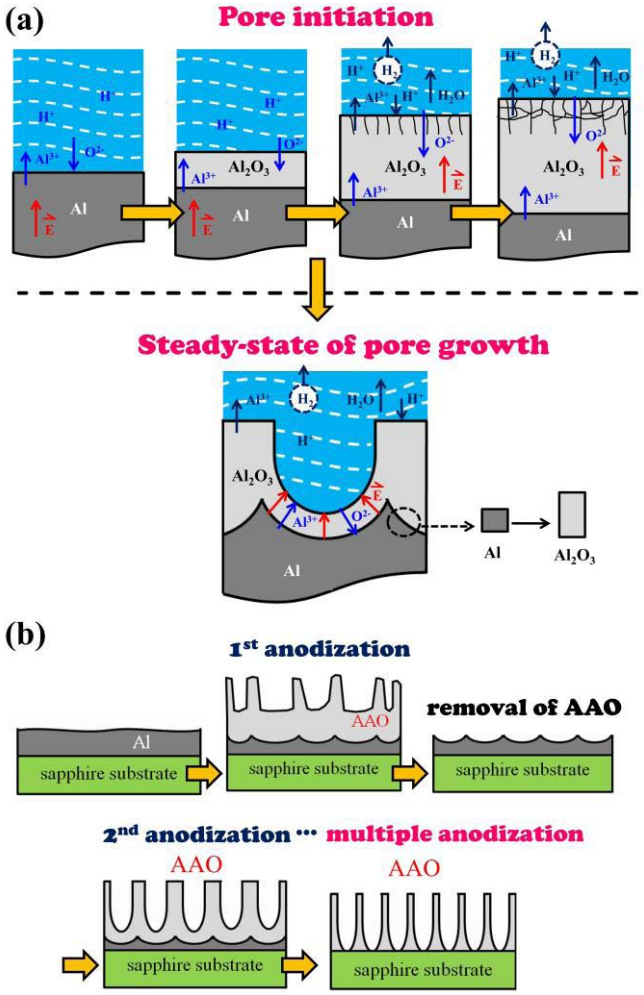

Fig. 2. (a) Anodization reaction procedures of AAO thin film grown on a sapphire substrate. (b) Schematic diagrams of the formation of a well-ordered AAO thin film by a multi-step anodization approach.

The optical characteristics were measured by an integrated sphere with a current source.

III. Results and Discussion

Figure 2(a) shows anodization reaction procedures of AAO thin film grown on a sapphire substrate. The AAO thin film growth mechanism could be divided into two parts including pore initiation and steady-state of pore growth [15]–[17].

A. Pore Initiation

(i) At the initiation of anodization, due to the electrical field in the electrolyte, Al ions are oxidized from Al film. Based on the cracking reaction at the Al film/water interface, oxygen ions are also pushed to the surface of Al film simultaneously. The related reactions could be expressed as:

$$Al_{(s)} \rightarrow Al^{3+}_{(aq)} + 3e^{-} \quad (1)$$

$$H_2O_{(l)} \rightarrow 2H^{+}_{(aq)} + O^{2-}_{(aq)} \quad (2)$$

(ii) Alumina is then formed on the surface of Al film. Therefore, due to the volume expansion of alumina, a higher electrical field is induced at concave surfaces and results in the penetration path. The local field strength at penetration paths is increased, which enhances the development of penetration paths through field-assisted dissolution. The higher electrical field accelerates this reaction and forms initial hemisphere holes at the surface of Al film as expressed in the following:

$$2Al^{3+}_{(aq)} + 3O^{2-}_{(aq)} \rightarrow Al_2O_{3(s)} \quad (3)$$

(iii) The generated alumina also reacts with hydrogen ions in the electrolyte. Thus, alumina is dissolved in the electrolyte simultaneously. Yet, only around 30% alumina is consumed in this reaction. 70% alumina is still remained in the end of reaction [16]. Parts of hydrogen ions are also combined with electrons. Hence, hydrogen gas would be produced around the cathode [16]:

$$Al_2O_{3(s)} + 6H^{+}_{(aq)} \rightarrow 2Al^{3+}_{(aq)} + 3H_2O_{(l)} \quad (4)$$

$$2H^{+}_{(aq)} + 2e^{-} \rightarrow H_{2(g)} \quad (5)$$

B. Steady-State of Pore Growth

Due to the formation of concave pores, the electrical field is preferably concentrated at the bottom of these concave pores and results in the accelerated alumina dissolution. At the same time, Al ions could be oxidized from Al film. Finally, these two reactions develop a dynamic equilibrium state. The barrier layer, which is at the bottom of alumina layer, maintains a constant thickness and grows downward stably. The concave-hemisphere shape of barrier layer is caused by mechanical stress resulted from the formation of AAO at metal/oxide interface with different expansion coefficients [17]. With increasing the growth time, stresses between neighboring pores push each other, which results in a gradually regular and honeycomb-like arrangement. Afterwards, the formation of cylindrical pores with a self-organized hexagonal arrangement could be observed. Notably, after the first anodization and the removal of alumina layer by a NaOH solution, ordered hemisphere-shaped concaves could be left on the surface. These ordered concaves could be served as seeds for the pore nucleation of second-time anodization. Thus, a well-ordered AAO thin film could be formed by a multi-step anodization approach as shown in Fig. 2(b) [16].

Figure 3(a) shows scanning electron microscope (SEM) images of AAO thin films grown on a sapphire substrate by a one-step anodization approach with 0, 10, 20, 30, 40, and 50 minutes pore widening times, respectively. A 0.3 M oxalic acid solution at 4 °C was used as the electrolyte. The bias voltage was 40 V and anodization time was 90 minutes. After anodization, the diameter of pores was too small to be used in device applications. In addition, the rate of dissolution of alumina layer is too rapid to control the pore widening by using a NaOH solution. Hence, an H_3PO_4 solution was employed to widen these pores. Empirically, the relationship between pore widening time x (minute) and pore diameters y (nm) is $y = 21.96 + 0.91x$ [14]. As expected, the diameter

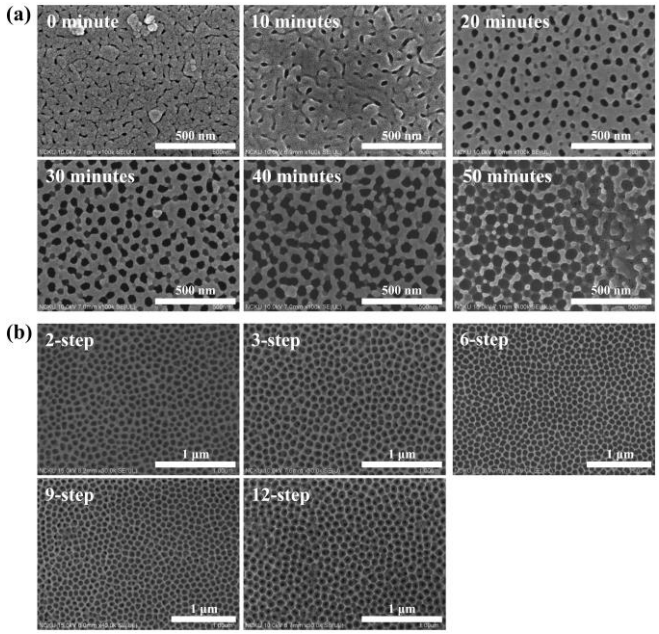

Fig. 3. (a) SEM images of AAO thin films grown on a sapphire substrate by an one-step anodization approach with 0, 10, 20, 30, 40, and 50 minutes pore widening times. (b) SEM images of AAO thin films grown on a sapphire substrate by two, three, six, nine, and twelve-step anodizations.

of pores could be increased after 30 minutes pore widening. However, part of walls between pore and pore appear to be over etched and broken after 30 minutes pore widening. The shape and arrangement of pores are also irregular. Therefore, a three-step approach was introduced in this work to obtain a more orderly AAO thin film with widened pores. Figure 3(b) shows SEM images of AAO thin films grown on a sapphire substrate by two, three, six, nine, and twelve-step anodizations, respectively. In the interval of two anodizations, the resulting alumina layer was removed by treating with a 0.5 M NaOH solution for 1 minute. Obviously, as compared with the two-step anodization, the AAO thin film after three-step anodizations is more regular and uniform. Experimentally, regularities of AAO thin films by six, nine, and twelve-step anodizations are similar with that by a three-step one. It could be observed that the influence of repetition of anodization is only apparent in initial times. Since pore regularity has been improved in initial anodizations, the improved pore regularity of AAO thin films after more than three-step anodizations is negligible.

SEM images on top and cross-section views of a self-assembled SiO_2 nanosphere monolayer and a well-ordered AAO thin film on a sapphire substrate are shown in Figs. 4(a) and 4(b). This 100 ± 5 nm SiO_2 nanosphere monolayer exhibits a pseudo-hexagonal close packing arrangement [18]. In addition, the mean diameter and depth of nanopores on the AAO thin film are 60 ± 3 and 770 ± 10 nm, respectively. Obviously, these nanopores on AAO thin film also exhibit a high aspect ratio and a well-ordered self-aligned arrangement. SEM images of tilt view of nanocomb-shaped and nanohemisphere-shaped PSSs are shown in Figs. 4(c) and 4(d). The mean diameter of nanopores (nanohemisphere) on the nanocomb-shaped (nanohemisphere-

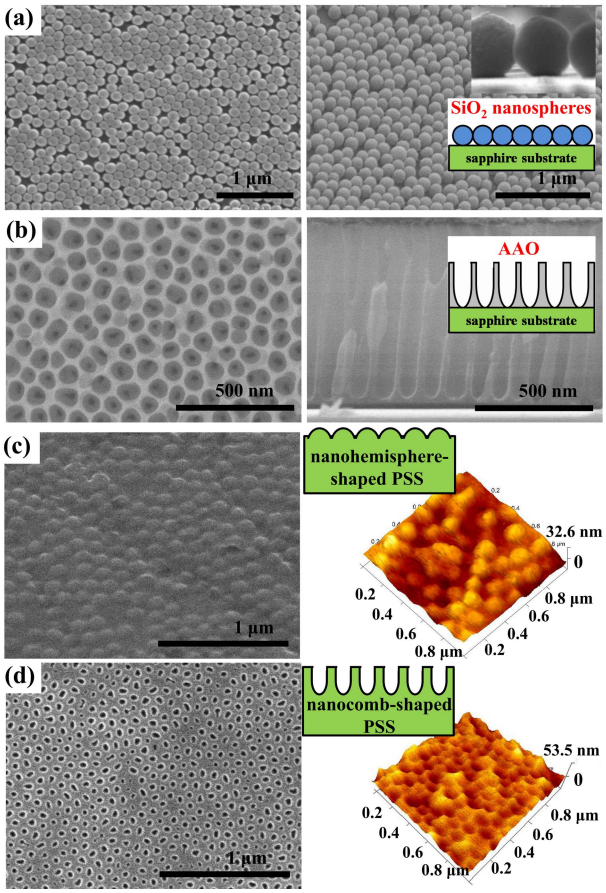

Fig. 4. Top and cross-section views of SEM images of (a) a SiO_2 nanosphere monolayer and (b) an AAO thin film on sapphire substrates. SEM and AFM images of surface morphology of (c) nanohemisphere-shaped and (d) nanocomb-shaped PSSs.

shaped) PSSs is 50 ± 3 (80 ± 4) nm. The mean depth of these nanopores (nanohemisphere) is 130 ± 2 (20 ± 2) nm. As compared with mean diameters and depths of nanopores on AAO thin film and SiO_2 nanospheres, smaller diameters and depths of nanopore and nanohemisphere patterns on nanocomb-shaped and nanohemisphere-shaped PSSs could be developed by the presence of concave hemisphere-shaped AAO barrier layer and different ICP etching rates between SiO_2 and sapphire as well as between AAO and sapphire [19]. Atomic force microscopy (AFM) images of surface morphology of nanocomb-shaped and nanohemisphere-shaped PSSs are also shown in Figs. 4(c) and 4(d). Root-mean-square values in AFM analyses of nanocomb-shaped and nanohemisphere-shaped PSSs are 6.5 ± 0.7 and 4.4 ± 0.4 nm, respectively. These results indicate that nanopore and nanohemisphere patterns could both be formed in a large area with a well-ordered arrangement on a sapphire substrate by using an AAO thin film and SiO_2 nanospheres as etching masks. Moreover, due to the feature of high aspect ratio, an AAO thin film could be operated with a longer time under the ICP dry etching ambience as compared with the SiO_2 nanosphere monolayer. Thus, a nanocomb-shaped PSS with a higher roughness morphology could be achieved by the use of a high aspect ratio AAO thin film as an etching mask. In addition, a nominal continuous

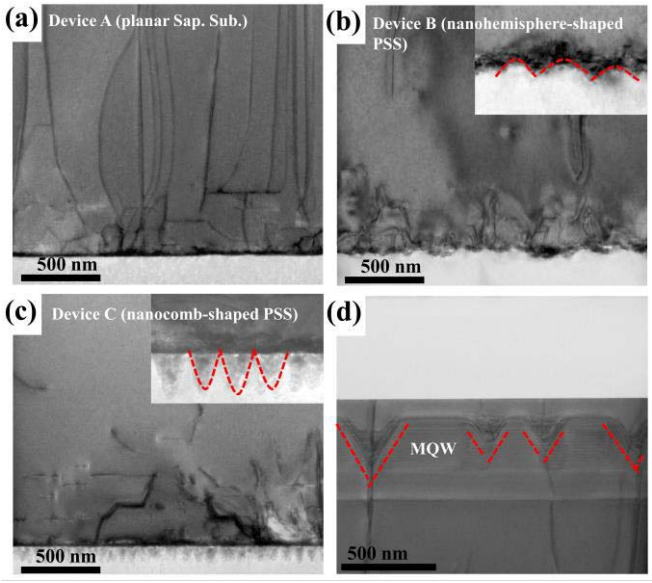

Fig. 5. TEM images of cross-section view of devices (a) A, (b) B, and (c) C. (d) V-shaped pits would be formed in the MQW as the apex of TDs.

variation of filling fraction could be observed to form a PhC-like air buffer layer. This PhC-like structure could enhance light scattering effect or reflect photons as a photonic band gap [11]. Thus, photons reflected upward the top side could be scattered by this PhC-like air buffer layer rather than be consumed by Fresnel losses and absorption of package metal [20]. Thus, photons originally emitted out of escape cones could be redirected back into these escape cones on the top of device and result in a higher LEE.

Figures 5(a), 5(b), and 5(c) show transmission electron microscopy (TEM) images of cross-section views of devices A, B, and C, respectively. The insets reveal enlarged views of TEM images. It could be directly observed that TDs in the device A grow from the GaN/sapphire substrate interface and propagate to the upper GaN epitaxial layer. These TDs in the GaN epitaxial layer act as non-radiative recombination centers and leakage pathways, which effectively degrade the performance of GaN-based LEDs [7]. In addition, some V-shaped pits are formed in the multiple quantum well (MQW) as the apex of TDs as shown in Fig. 5(d). These V-shaped hexagonal pits cause the indium incorporation and a strongly inhomogeneous composition [21]. Although the indium incorporation around pits lead to a higher potential barrier, which blocks carriers from the occurrence of non-radiative recombination, these pits should still be reduced to maximize the light emitting area [21]. On the other hand, as shown in Figs. 5(b) and 5(c), the use of nanocomb-shaped and nanohemisphere-shaped PSSs could effectively reduce the propagation of TDs.

To confirm the enhanced crystalline quality, the related X-ray diffraction (XRD) rocking curves, photoluminescence (PL), and Raman spectra are shown in Figs. 6(a)–(c), respectively. It is known that the full width at half maximum (FWHM) of (0002) 2θ-ω scan XRD rocking curve could be used as an indicator of screw, edge, and mixed type dislocations [22]. Experimentally, (0002) diffraction-

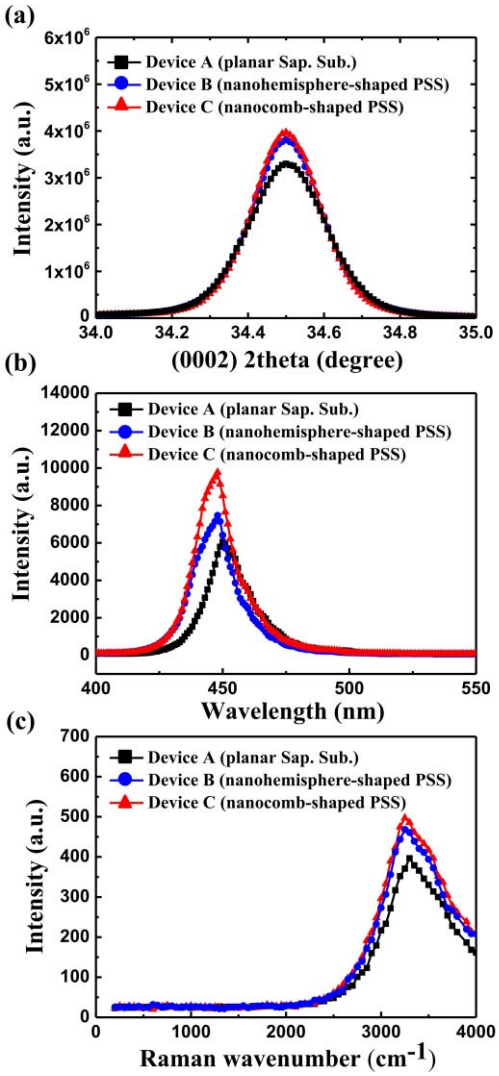

Fig. 6. (a) XRD rocking curves, (b) PL, and (c) Raman spectra of devices A, B, and C.

peak positions are same for all studied devices, but FWHM values of devices B (0.22 degree) and C (0.22 degree) are smaller than that of the device A (0.24 degree). This result indicates that dislocations in devices B and C are less than those in the device A. The PL spectrum measurement was excited by a 325 nm of He-Ne laser. Maximum intensities of devices B and C are 19.9 and 59.3% higher than that of the device A. As compared with the device A, FWHM values of devices B and C shrink from 22 (device A) to 21 (device B) and 20 nm (device C). These results reveal that the use of nanocomb-shaped and nanohemisphere-shaped PSSs could release the residual strain and reduce the piezoelectric field in GaN epitaxial layer [23]. Thus, the electron-hole pair recombination efficiency in the MQW could be enhanced [7]. Notably, PL spectra of devices B and C also show a blueshift phenomenon from 450 (device A) to 448 nm (devices B and C). This result indicates that the dislocation density could be reduced and the stress could be relaxed [23]. To further study the stress relaxation, the Raman spectrum measurement is also introduced. Experimentally, peak intensities of devices A, B, and C are about 396, 468, and 497 a.u., respectively, as shown

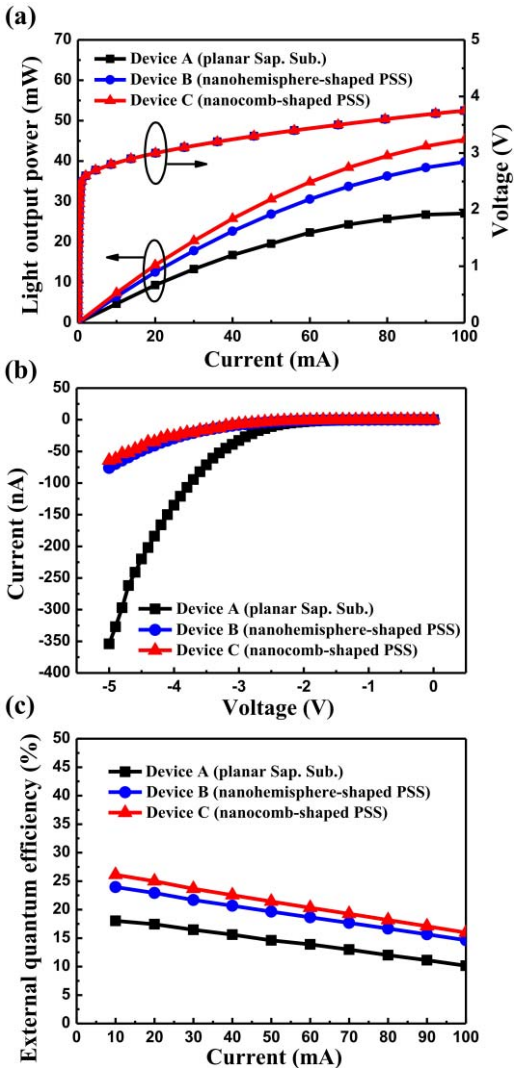

Fig. 7. (a) L-I-V curves, (b) Reverse leakage currents, and (c) EQEs of devices A, B, and C.

in Fig. 6(c). It is worthy to noted that peak wavenumbers of devices B and C also show a blueshift phenomenon from 3347 (device A) to 3262 (device B) and 3216 (device C) cm^{-1}. The stress in hetero-epitaxial layers could be estimated by $\sigma_{GaN} = \Delta\omega/6.2$, where σ_{GaN} is the biaxial compressive stress (in GPa) and $\Delta\omega$ is the frequency shift (in cm^{-1}) [7]. As compared with the device A, stress relaxations of devices B and C could be up to 13.7 and 21.1 GPa. These results demonstrate that strain state generated during epitaxial growth could be alleviated by the use of nanocomb-shaped and nanohemisphere-shaped PSSs, which certainly enhance crystalline quality of GaN-based LEDs.

Luminance-current-voltage (L-I-V) curves of devices A, B, and C are shown in Fig. 7(a). Experimentally, similar forward voltages of devices A, B, and C, at 20 mA, around 3 V are obtianed. Light output powers (LOPs) of devices A, B, and C, at 20 mA, are 9.3, 12.6, and 14.3 mW, respectively. As compared with the device A, devices B and C exhibit 35.5 and 53.8% improvements in LOP. Figure 7(b) shows measured reverse leakage currents of studied devices. Under a reverse operation voltage of 5 V, reverse-biased

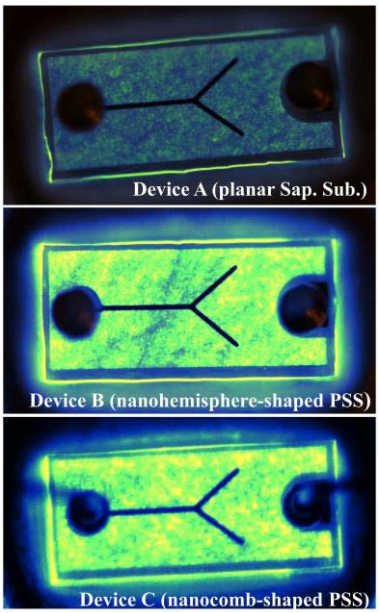

Fig. 8. EL emission optical microscopic images of devices A, B, and C at a low injection current of 0.03 mA.

leakage currents of devices A, B, and C are 354, 76, and 64 nA, respectively. The reduced leakage currents could be attributed to the use of nanocomb-shaped and nanohemisphere-shaped PSSs to effectively reduce the presence of TDs. These TDs could provide leakage pathways for electron-hole pairs to pass through active region [7]. In addition, as compared with the device B, better crystalline quality of the device C might be attributed the higher roughness of nanocomb-shaped PSS, which could result in more bending and annihilation of TDs [24]. Thus, the presence of TDs could be suppressed more validly. Figure 7(c) shows EQEs as a function of operation current of devices A, B, and C. EQEs of devices A, B, and C, at 20 mA, are 17.4%, 22.9%, and 25.0%, respectively. As compared with the device A, devices B and C exhibit 31.6 and 43.7% enhancements in EQE. Since PSS could restrict the presence of strain, the reduction of TD density caused by stress relaxation could be achieved [7]. The decrease of non-radiative recombination caused by the reduction of TD density certainly leads to an increase in IQE [7]. Additionally, the light scattering effect could also be enhanced. Thus, photons emitted out of escape cones could be redirected back into these escape cones on the top of device and result in a higher LEE. Notably, as compared with the device B, better optical performance of the device C could be attributed to the formation of PhC-like air buffer layer between the GaN epitaxial layer and the nanocomb-shaped PSS. Due to the change of refractive indices, photons reflected upward the top side could be scattered by this layer [11]. Therefore, more photons could be extracted outside. This result indicates that the AAO thin film with a high aspect ratio is more suitable for the fabrication. Electroluminescence emission optical microscopic images of devices A, B, and C, at a low injection current of 0.03 mA, are shown in Fig. 8. As expected, devices B and C both show the brighter and more uniform emission performance as compared with the device A. These significant improved

electrical and optical properties show that high-efficiency GaN-based LEDs could be achieved by the employment of nanocomb-shaped PSS.

IV. Conclusion

A GaN-based LED grown on a nanocomb-shaped PSS is fabricated and studied. Nanocomb-shaped patterns are transferred on a sapphire substrate by using a large-area self-organized AAO thin film as a mask for the ICP dry etching process. This well-ordered AAO thin film with a high aspect ratio is grown on a sapphire substrate by an oxalic acid-based electrochemical system and a three-step anodization. The growth mechanism of AAO thin film is also demonstrated in this study. The mean diameter and depth of nanopores on the nanocomb-shaped PSS are 50 ± 3 and 130 ± 2 nm, respectively. Experimentally, due to the use of nanocomb-shaped PSS, the strain generated during epitaxial growth could be relaxed. The presence of TDs, which act as non-radiative recombination centers and leakage pathways, could be effectively reduced. Thus, IQE of the studied LED could be enhanced. Notably, after XRD, PL, and Raman measurements, as compared with LEDs grown on a conventional planar sapphire substrate, the studied LED exhibits better crystalline quality. 21.1GPa stress relaxation could also be obtained. These results are mainly caused by the higher roughness of nanocomb-shaped PSS, which result in the more bending and annihilation of TDs. In addition, due to the presence of PhC-like air buffer layer, photons reflected upward the top side could be scattered by this layer rather than be consumed by Fresnel losses and absorption. Therefore, LEE of the studied LED could also be enhanced. At 20 mA, as compared with a conventional LED grown on a planar sapphire substrate, the studied LED grown on a nanocomb-shaped PSS shows a reduced leakage current as well as 53.8 and 43.7% enhancements in LOP and EQE. These significant improved electrical and optical properties show that high-performance GaN-based LEDs could be achieved by the employment of nanocomb-shaped PSS.

References

[1] W.-C. Yang, C. Lo, C.-Y. Wei, and W.-S. Lour, "Cell-temperature determination in InGaP–(In)GaAs–Ge triple-junction solar cells," *IEEE Electron Device Lett.*, vol. 32, no. 10, pp. 1412–1414, Oct. 2011.

[2] D.-F. Guo, "A new AlGaAs/GaAs/InAlGaP npn bulk-barrier optoelectronic switch," *IEEE Electron Device Lett.*, vol. 24, no. 3, pp. 162–164, Mar. 2003.

[3] T.-B. Wang *et al.*, "Single-mode InGaAs photonic crystal vertical-cavity surface-emitting lasers emitting at 1170 nm," *J. Electrochem. Soc.*, vol. 154, no. 5, pp. H351–H353, Mar. 2007.

[4] I. Schnitzer, E. Yablonovitch, C. Caneau, T. J. Gmitter, and A. Scherer, "30% external quantum efficiency from surface textured, thin-film light-emitting diodes," *Appl. Phys. Lett.*, vol. 63, no. 16, pp. 2174–2176, Aug. 1993.

[5] Y.-L. Chou *et al.*, "Improvement of surface emission for GaN-based light-emitting diodes with a metal-via-hole structure embedded in a reflector," *IEEE Photon. Technol. Lett.*, vol. 23, no. 7, pp. 393–395, Apr. 1, 2011.

[6] J.-K. Liou *et al.*, "Effects of the use of an aluminum reflecting and an SiO_2 insulating layers (RIL) on the performance of a GaN-based light-emitting diode with the naturally textured p-GaN surface," *IEEE Trans. Electron Devices*, vol. 60, no. 7, pp. 2282–2289, Jul. 2013.

[7] T. Kozawa, T. Kachi, H. Kano, H. Nagase, N. Koide, and K. Manabe, "Thermal stress in GaN epitaxial layers grown on sapphire substrates," *J. Appl. Phys.*, vol. 77, no. 9, pp. 4389–4392, May 1995.

[8] D. Deng *et al.*, "InGaN-based light-emitting diodes grown and fabricated on nanopatterned Si substrates," *Appl. Phys. Lett.*, vol. 96, no. 20, pp. 201106-1–201106-3, May 2010.

[9] C. Geng *et al.*, "Fabrication of volcano-shaped nano-patterned sapphire substrates using colloidal self-assembly and wet chemical etching," *Nanotechnology*, vol. 24, no. 33, p. 335301, Jul. 2013.

[10] C.-H. Chiu *et al.*, "Light extraction enhancement of GaN-based light-emitting diodes using crown-shaped patterned sapphire substrates," *IEEE Photon. Technol. Lett.*, vol. 24, no. 14, pp. 1212–1214, Jul. 15, 2012.

[11] Y. K. Su, J. J. Chen, C. L. Lin, S. M. Chen, W. L. Li, and C. C. Kao, "GaN-based light-emitting diodes grown on photonic crystal-patterned sapphire substrates by nanosphere lithography," *Jpn. J. Appl. Phys.*, vol. 47, no. 8S1, pp. 6706–6708, Aug. 2008.

[12] N. Okada *et al.*, "InGaN-based light-emitting diodes fabricated on nano patterned sapphire substrates with pillar height of more than 600 nm by nanoimprint lithography," *Jpn. J. Appl. Phys.*, vol. 52, no. 11S, p. 11NG02, Nov. 2013.

[13] Z.-J. Tsai, J.-K. Liou, and W.-C. Liu, "Enhanced performance of a GaN-based LED prepared by an anodized aluminum oxide-nanoporous pattern sapphire substrate," *IEEE Electron Devices Lett.*, vol. 34, no. 7, pp. 909–911, Jul. 2013.

[14] A. P. Li, F. Müller, A. Birner, K. Nielsch, and U. Gösele, "Hexagonal pore arrays with a 50–420 nm interpore distance formed by self-organization in anodic alumina," *J. Appl. Phys.*, vol. 84, no. 11, pp. 6023–6026, Dec. 1998.

[15] G. E. Thompson, "Porous anodic alumina: Fabrication, characterization and applications," *Thin Solid Films*, vol. 297, nos. 1–2, pp. 192–201, Apr. 1997.

[16] F. Li, L. Zhang, and R. M. Metzger, "On the growth of highly ordered pores in anodized aluminum oxide," *Chem. Mater.*, vol. 10, no. 9, pp. 2470–2480, Aug. 1998.

[17] O. Jessensky, F. Müller, and U. Gösele, "Self-organized formation of hexagonal pore arrays in anodic alumina," *Appl. Phys. Lett.*, vol. 72, no. 10, pp. 1173–1175, Mar. 1998.

[18] Y.-C. Chang, J.-K. Liou, and W.-C. Liu, "Improved light extraction efficiency of a high-power GaN-based light-emitting diode with a three-dimensional-photonic crystal (3-D-PhC) backside reflector," *IEEE Electron Devices Lett.*, vol. 34, no. 6, pp. 777–779, Jun. 2013.

[19] B.-J. Kim *et al.*, "Inductively coupled plasma etching of nano-patterned sapphire for flip-chip GaN light emitting diode applications," *Thin Solid Films*, vol. 516, no. 21, pp. 7744–7747, Sep. 2008.

[20] T.-X. Lee, K.-F. Gao, W.-T. Chien, and C.-C. Sun, "Light extraction analysis of GaN-based light-emitting diodes with surface texture and/or patterned substrate," *Opt. Exp.*, vol. 15, no. 11, pp. 6670–6676, May 2007.

[21] Y.-H. Cho *et al.*, "Quantum efficiency affected by localized carrier distribution near the V-defect in GaN based quantum well," *Appl. Phys. Lett.*, vol. 103, no. 26, pp. 261101-1–261101-4, Dec. 2013.

[22] B. Heying *et al.*, "Role of threading dislocation structure on the X-ray diffraction peak widths in epitaxial GaN films," *Appl. Phys. Lett.*, vol. 68, no. 5, pp. 643–645, Jan. 1996.

[23] C.-Y. Hsieh, B.-W. Lin, H.-J. Cho, B.-M. Wang, N. Chang, and Y.-C. S. Wu, "Improvement of epitaxy GaN quality using liquid-phase deposited nano-patterned sapphire substrates," *IEEE Photon. Technol. Lett.*, vol. 24, no. 24, pp. 2232–2234, Dec. 15, 2012.

[24] W. Zhou, D. Ren, and P. D. Dapkus, "Transmission electron microscopy study of defect reduction in two-step lateral epitaxial overgrown non-planar GaN substrate templates," *J. Cryst. Growth*, vol. 290, no. 1, pp. 11–17, Apr. 2006.

Jian-Kai Liou was born in Taichung, Taiwan, in 1987. He received the B.S. degree from the Department of Electronic Engineering, National Kaohsiung Normal University, Kaohsiung, Taiwan, in 2010. He is currently pursuing the Ph.D. degree with the Department of Electrical Engineering, Institute of Microelectronics, National Cheng Kung University, Tainan, Taiwan. His research has focused on the III–V compound light-emitting diodes.

Chun-Chia Chen was born in Changhua, Taiwan, in 1986. He received the B.S. degree from the Department of Electronic Engineering, Feng Chia University, Taichung, Taiwan, in 2008. He is currently pursuing the Ph.D. degree with the Department of Electrical Engineering, Institute of Microelectronics, National Cheng Kung University, Tainan, Taiwan. His research has focused on III–V heterostructure field-effect transistors.

Po-Cheng Chou was born in Tainan, Taiwan, in 1988. He received the B.S. degree in electrical engineering from I-Shou University, Kaohsiung, Taiwan, in 2010. He is currently pursuing the Ph.D. degree with the Department of Electrical Engineering, Institute of Microelectronics, National Cheng Kung University, Tainan, Taiwan. His research has focused on semiconductor gas sensors.

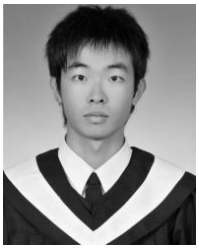

Zong-Jie Tsai was born in Taipei, Taiwan, in 1990. He received the B.S. and M.S. degrees from the Department of Electrical Engineering, Institute of Microelectronics, National Cheng Kung University, Tainan, Taiwan, in 2012 and 2013, respectively. His research has focused on the III–V compound light-emitting diodes.

Yu-Chih Chang was born in Taichung, Taiwan, in 1987. He received the B.S. degree from the Department of Electronic Engineering, Feng Chia University, Taichung, Taiwan, in 2009. He is currently pursuing the M.S. degree with the Department of Electrical Engineering, Institute of Microelectronics, National Cheng Kung University, Tainan, Taiwan. His research has focused on the III–V compound light-emitting diodes.

Wen-Chan Liu (A'91–M'93–SM'02) received the B.S., M.S., and Ph.D. degrees from the Department of Electrical Engineering, National Cheng Kung University, Tainan, Taiwan, in 1979, 1981, and 1986, respectively, where he has been a Professor since 1992. His current research interests include compound semiconductor-based sensors, electronic, and photonic devices.